Synthesis, Crystal Structures, and Some Properties of S-Bridged Pt(II)–M(III) (M = Co, Rh) Dinuclear Complexes with Square-Planar and Octahedral Geometries

Yasunori Yamada,* Mamoru Uchida, Yoshitaro Miyashita, Kiyoshi Fujisawa, Takumi Konno,† and Ken-ichi Okamoto*

Department of Chemistry, University of Tsukuba, Tsukuba, Ibaraki 305-8571

†Department of Chemistry, Faculty of Engineering, Gunma University, Kiryu, Gunma 376-8516

(Received October 27, 1999)

A novel dinuclear complex $[\{Pt(bpy)\}\{Co(aet)_2(en)\}]^{3+}$ (bpy = 2,2′-bipyridine; aet = 2-aminoethanethiolate; en = ethylenediamine) (**1**) composed of square-planar and octahedral geometries was obtained by a substitution reaction of $[Ni\{Co(aet)_2(en)\}_2]^{4+}$ with $[PtCl_2(bpy)]$. The reactions of *fac*(*S*)-$[M(aet)_3]$ ($M = Co^{III}$, Rh^{III}) with $[PtCl_2(bpy)]$ also gave a similar type of S-bridged dinuclear complexes $[\{Pt(bpy)\}\{M(aet)_3\}]^{2+}$ ($M = Co^{III}$ (**2**), Rh^{III} (**3**)). The crystal structures of complexes **1**, **2**, and **3** were determined by X-ray crystallography. All of the Co and Rh atoms in **1**, **2**, and **3** take approximately octahedral geometry. The Pt atoms in **1**, **2**, and **3** are coordinated by two N atoms in bpy and two S atoms from C_2-*cis*(*S*)-$[Co(aet)_2(en)]^+$ or $[M(aet)_3]$ unit, and all of them take square-planar geometry. *fac*(*S*)-$[Co(aet)_3]$ is structurally converted into a *mer*(*S*)-$[Co(aet)_3]$ unit during the course of producing a $[\{Pt(bpy)\}\{M(aet)_3\}]^{2+}$-type dinuclear complex, although *fac*(*S*)-$[Rh(aet)_3]$ retains its structure. These complexes were characterized on the basis of the electronic absorption, CD, and ^{13}C NMR spectra, together with cyclic voltammetry.

It has been recognized that the reactions of the square-planar $[M'(aet)_2]$ (M' = Ni^{II} or Pd^{II}, aet = 2-aminoethanethiolate), which can function as metalloligand including two bridging S-atoms, with a square-planar metal ion or its complex give S-bridged polynuclear complexes comprising square-planar units.[1—5] For instance, the reaction of $[Ni(aet)_2]$ with Pd^{2+} ion gave stereoselectively a pin-wheel-type S-bridged hexanuclear complex, $[Pd_2\{Ni(aet)_2\}_4]^{4+}$, in which all of the Pd^{2+} and Ni^{2+} ions take square-planar geometries.[4] In the case of the reaction of $[Pd(aet)_2]$ with $[Pd(NO_3)_2(bpy)]$ (bpy = 2,2′-bipyridine), in which the ligand bpy is less susceptible to substitution of other ligands, an S-bridged tetranuclear complex, $[\{Pd(bpy)\}_2\{Pd(aet)_2\}_2]^{4+}$, was formed.[5] As for the construction and properties of S-bridged polynuclear complexes including square-planar metal ions and $[M'(aet)_2]$ units, significant information has been obtained so far. On the other hand, the octahedral *fac*(*S*)-$[M(aet)_3]$ ($M = Co^{III}$, Rh^{III}, or Ir^{III}) reacts with a square-planar metal ion to form intricate polynuclear structures comprising square-planar and octahedral units.[6,7] From a reaction between *fac*(*S*)-$[M(aet)_3]$ ($M = Rh^{III}$ and Ir^{III}) and Pd^{2+} ion, for instance, the pentanuclear complexes, $[Pd\{Pd(aet)\}\{M(aet)_2\}\{M(aet)_3\}_2]^{4+}$, were produced.[7] Though several types of polynuclear complexes with square-planar and octahedral geometries were obtained by the reaction of *fac*(*S*)-$[M(aet)_3]$ with a square-planar metal ion, details of their formation mechanism and properties remain equivocal. In order to know more detailed information about S-bridged polynuclear complexes with square-planar and octahedral geometries, it seems profitable to examine the reaction of *fac*(*S*)-$[M(aet)_3]$ with $[PtCl_2(bpy)]$, and to clarify the structures and properties of the resulting complexes. While the S-donating metalloligand, *fac*(*S*)-$[M(aet)_3]$, has three effective S atoms for bridging another metal, it is expected to act as a bidentate ligand toward $[PtCl_2(bpy)]$ with two chloride ligand susceptible to substitution of other ligands and produce the $[\{Pt(bpy)\}\{M(aet)_3\}]^{2+}$ type S-bridged dinuclear complex. In the present paper, we report on the syntheses, structures, and chemical characterizations of the S-bridged dinuclear complexes, $[\{Pt(bpy)\}\{M(aet)_3\}]^{2+}$ ($M = Co^{III}$ and Rh^{III}). Further, the dinuclear complex, $[\{Pt(bpy)\}\{Co(aet)_2(en)\}]^{3+}$ (en = ethylenediamine), whose structure is expected to be similar to $[\{Pt(bpy)\}\{Co(aet)_3\}]^{2+}$, was prepared by the substitution reaction[8—10] of $[Ni\{Co(aet)_2(en)\}_2]^{4+}$ with $[PtCl_2(bpy)]$. The properties of the obtained complexes are also discussed in comparison with those of the corresponding complexes.

Experimental

Materials. $RhCl_3 \cdot nH_2O$ and K_2PtCl_4 were purchased from N. E. Chemcat Co., Ltd., and Tanaka Rare Metal Industries Ltd., respectively. $[PtCl_2(bpy)]$,[11,12] $[Ni\{Co(aet)_2(en)\}_2]Cl_4 \cdot 6H_2O$,[8] *fac*(*S*)-$[Co(aet)_3]$,[2] and *fac*(*S*)-$[Rh(aet)_3]$[13—15] were prepared by modified methods from the literature. $Na_2[Sb_2(d\text{-tartrato})_2] \cdot 5H_2O$ was prepared from Na(*d*-H_3tartrato)$\cdot H_2O$ and Sb_2O_3. The other chemicals were obtained from Wako Pure Chemical Ind., Co., Ltd., and Tokyo Chemical Co., Ltd. All of the chemicals were

of reagent grade and were used without further purification.

Preparation of Complexes. [Pt(bpy){Co(aet)$_2$(en)}]$^{3+}$ (1). To a brown solution containing 0.090 g (0.11 mmol) of [Ni{Co(aet)$_2$(en)}$_2$]Cl$_4$·6H$_2$O[8] in 10 cm^3 of water was added 0.089 g (0.21 mmol) of [PtCl$_2$(bpy)].[11,12] The mixture was stirred at 60 °C for 1 h, whereupon the mixture became a red solution. After removing any unreacted materials by filtration, 1.0 cm^3 of a saturated NaNO$_3$ solution was added to the red filtrate. The mixture was allowed to stand at 4 °C for 1 d, and the resulting reddish-pink crystals were collected by filtration. A well-formed crystal of **1**·(NO$_3$)$_3$·1.75H$_2$O was used for an X-ray structural analysis. Yield: 0.078 g (44%). Calcd for [Pt(bpy){Co(aet)$_2$(en)}]-(NO$_3$)$_3$·1.75H$_2$O = C$_{16}$H$_{31.5}$N$_9$O$_{10.75}$S$_2$CoPt: C, 22.86; H, 3.78; N, 15.00%. Found: C, 22.63; H, 3.67; N, 14.91%.

[Pt(bpy){Co(aet)$_3$}]$^{2+}$ (2). To a suspension containing 0.27 g (0.95 mmol) of *fac*(*S*)-[Co(aet)$_3$][2] in 30 cm^3 of water was added 0.41 g (0.96 mmol) of [PtCl$_2$(bpy)].[11,12] The mixture was stirred at room temperature for 4 h, whereupon the mixture became a brown solution. After removing any unreacted materials by filtration, the brown filtrate was poured onto an SP-Sephadex C-25 column (Na$^+$ form, 5.0 cm×40 cm). After the column had been swept with water, the adsorbed band was eluted with a 0.20 mol dm^{-3} aqueous solution of sodium nitrate. Only a reddish-brown eluate was concentrated to a small volume with a rotary evaporator, and then left standing at room temperature overnight. The resulting reddish-brown crystals were collected by filtration. A well-formed crystal of **2**·(NO$_3$)$_2$·1.5H$_2$O was used for the X-ray structural analysis. Yield: 0.165 g (21%). Calcd for [Pt(bpy){Co(aet)$_3$}](NO$_3$)$_2$·1.5H$_2$O = C$_{16}$H$_{29}$N$_7$O$_{7.5}$S$_3$CoPt: C, 24.34; H, 3.70; N, 12.42%. Found: C, 24.25; H, 3.64; N, 12.32%.

[Pt(bpy){Rh(aet)$_3$}]$^{2+}$ (3). To a suspension containing 0.33 g (1.0 mmol) of *fac*(*S*)-[Rh(aet)$_3$][13—15] in 40 cm^3 of water was added 0.42 g (1.0 mmol) of [PtCl$_2$(bpy)].[11,12] The mixture was stirred at room temperature for 8 h, whereupon the mixture became an orange solution. After removing any unreacted materials by filtration, 25 drops of a saturated NaBr solution were added to the orange filtrate. The mixture was allowed to stand at room temperature for 5 d, and the resulting orange crystals were collected by filtration. A well-formed crystal of **3**·Br$_2$·5.5H$_2$O was used for X-ray structural analysis. Yield: 0.29 g (31%). Calcd for [Pt(bpy){Rh(aet)$_3$}]Br$_2$·5.5H$_2$O = C$_{16}$H$_{37}$N$_5$O$_{5.5}$S$_3$Br$_2$RhPt: C, 21.42; H, 4.16; N, 7.80%. Found: C, 21.78; H, 4.05; N, 7.54%.

[Pt(bpy){Co(aet)$_2$(smaet)}]$^{3+}$ (4; smaet = *S*-methyl-2aminoethanethiolate). To a purple solution containing 0.499 g (0.6 mmol) of **2**·(NO$_3$)$_2$·1.5H$_2$O in 30 cm^3 of water was added 0.3 cm^3 (ca. 3 mmol) of dimethyl sulfate. The mixture was stirred at room temperature for 20 min, whereupon the mixture became a red solution. After the solution was allowed to stand at room temperature overnight, any unreacted materials were removed by filtration. The red filtrate was poured onto an SP-Sephadex C-25 column (Na$^+$ form, 2.0 cm×30 cm). After the column had been swept with water, the adsorbed band was eluted with a 0.30 mol dm^{-3} aqueous solution of NaCl. Only the eluate was concentrated to dryness, and the residue was redissolved in a minimum amount of ethanol. After removing the insoluble NaCl by filtration, the filtrate was concentrated to dryness and the residue was dissolved in a small amount of water. To the solution was added 1.0 cm^3 of a saturated NaBr solution, and the mixture was allowed to stand at room temperature for 2 d. The resulting red crystals were collected by filtration. Yield; 0.45 g (66%). Calcd for [Pt(bpy){Co(aet)$_2$(smaet)}]-Br$_3$·4H$_2$O·1.5NaBr = C$_{17}$H$_{37}$N$_5$O$_4$Na$_{1.5}$S$_3$Br$_{4.5}$CoPt: C, 18.23; H, 3.33; N, 6.25%. Found: C, 18.03; H, 3.31; N, 6.05%.

Optical Resolution of Complexes. Each aqueous solution of complexes **1**, **2**, or **3** was poured onto an SP-Sephadex C-25 column (Na$^+$ form, 1.5 cm×60 cm). After the column had been swept with water, the adsorbed band was eluted with an aqueous solution of Na$_2$[Sb$_2$(*d*-tartrato)$_2$]·5H$_2$O (0.15 mol dm^{-3} for **1**, 0.075 mol dm^{-3} for **2** and **3**). When the adsorbed band was circulated in the same column twice, the band was completely separated into two bands. After complete separation into two bands, each band was eluted with an aqueous solution of NaCl (0.30 mol dm^{-3} for **1**, 0.15 mol dm^{-3} for **2** and **3**). It was found from absorption and CD spectral measurements that each band contained a Δ- or Λ-isomer of the complex. The concentration of each isomer was evaluated on the basis of the absorption spectrum of the racemic salt.

Measurements. The electronic absorption spectra were recorded with a JASCO Ubest V-560 or V-570 spectrophotometer, and the CD spectra with a JASCO J-600 spectropolarimeter. All of the measurements were carried out in aqueous solutions at room temperature. Electrochemical measurements were made with a CV-1B apparatus (Bioanalytical Systems, Inc.; BSI) using a glassy-carbon working electrode and a platinum microelectrode (BSI). An aqueous Ag/AgCl/NaCl (3 mol dm^{-3}) electrode (BSI) and a platinum wire were used as reference and auxiliary electrodes, respectively. Electrochemical experiments were conducted at room temperature in a 0.1 mol dm^{-3} aqueous solution of Na$_2$SO$_4$ as the supporting electrolyte and complex concentrations of 1.0 mmol dm^{-3}. The ^{13}C NMR spectra were recorded with a Bruker AM-500 NMR spectrometer in D$_2$O. The sodium 4,4-dimethyl-4-silapentane-1-sulfonate (DSS) was used as an internal reference. Elemental analyses (C, H, N) were performed by the Analysis Center of the University of Tsukuba.

Crystallography. The unit-cell parameters and intensity data for **1**·(NO$_3$)$_3$·1.75H$_2$O, **2**·(NO$_3$)$_2$·1.5H$_2$O, and **3**·Br$_2$·5.5H$_2$O were used for data collection on a Rigaku RASA-7S four-circle diffractometer with graphite-monochromatized Mo $K\alpha$ radiation. The unit-cell parameters were determined by a least-square refinement of 22 reflections for **1**·(NO$_3$)$_3$·1.75H$_2$O ($12.6° < \theta < 14.1°$), 25 reflections for **2**·(NO$_3$)$_2$·1.5H$_2$O ($14.3° < \theta < 14.9°$), and 20 reflections for **3**·Br$_2$·5.5H$_2$O ($14.4° < \theta < 15.0°$). The crystal data and experimental parameters are listed in Table 1. The intensity data were collected by the ω–2θ scan technique, and the intensities were corrected for Lorentz and polarization. An empirical absorption correction based on a series of Ψ scans was applied. The independent reflections with $I_0 > 2\sigma(I_0)$ were used for structure determinations. The positions of the Pt and other atoms were determined by a direct method. The difference Fourier maps based on these atomic positions revealed some remaining non-hydrogen atoms. The structures were refined by a full-matrix least-squares refinement on F of the positional parameters and the anisotropic thermal parameters of the non-hydrogen atoms in **1**·(NO$_3$)$_3$·1.75H$_2$O, **2**·(NO$_3$)$_2$·1.5H$_2$O, and **3**·Br$_2$·5.5H$_2$O. The hydrogen atoms on the ligands were fixed by the geometrical and thermal constrains (C–H = N–H = 0.95 Å and U = 1.3U (C, N). All of the calculations were performed on an Indigo II computer using teXsan.[16] The final atomic coordinates for non-hydrogen atoms are given in Tables 2, 3, and 4.[17] Crystallographic data have been deposited at the CCDC, 12 Union Road, Cambridge CB2 1EZ, UK and copies can be obtained on request, free of charge, by quoting the publication citation and the deposition numbers 139653-139655.

Results and Discussion

Syntheses. The trinuclear complex, [Ni{Co-

Table 1. Crystal Data of [Pt(bpy){Co(aet)$_2$(en)}](NO$_3$)$_3$·1.75H$_2$O (**1**), [Pt(bpy){Co(aet)$_3$}](NO$_3$)$_2$·1.5H$_2$O (**2**), and [Pt(bpy){Rh(aet)$_3$}]Br$_2$·5.5H$_2$O (**3**)

	1	**2**	**3**
Formula	$C_{16}H_{31.5}N_9O_{10.75}S_2CoPt$	$C_{16}H_{29}N_7O_{7.5}S_3CoPt$	$(C_{16}H_{37}N_5O_{5.5}S_3Br_2RhPt)_2$
Fw	840.12	789.65	1864.95
Cryst dimens / mm	0.50×0.10×0.05	0.03×0.20×0.35	0.35 × 0.10 × 0.10
Space group	*C*2/*c*	$P\bar{1}$	$P2_1/c$
a/Å	17.578(3)	11.849(3)	14.595(3)
b/Å	21.495(3)	14.444(3)	14.149(3)
c/Å	15.008(3)	7.899(1)	28.769(3)
α/deg		94.36(2)	
β/deg	107.78(1)	98.08(2)	99.74(1)
γ/deg		95.66(2)	
V/Å^3	5400(1)	1326.5(5)	5855(1)
Z	8	2	4
D_{calcd}/g cm^{-3}	1.989	1.977	2.115
μ/cm^{-1}	59.95	61.59	83.02
Transm factor	0.78—1.00	0.45—1.00	0.79—1.00
Scan type	ω–2θ	ω–2θ	ω–2θ
θ range/deg	55.0	55.0	55.3
No. of reflcns measd	6379	6391	13951
No. of reflcns used	4376	4514	7630
No. of variables used	366	325	613
R (R_w)	0.035 (0.044)	0.040 (0.049)	0.047 (0.062)

(aet)$_2$(en)}$_2$]$^{4+}$, reacts with [PtCl$_2$(bpy)] to form the novel S-bridged dinuclear complex, [Pt(bpy){Co(aet)$_2$(en)}]$^{3+}$ (**1**), including square-planar and octahedral geometries. The reactions of *fac*(*S*)-[M(aet)$_3$] (M = Co^{III} (**2**) or Rh^{III} (**3**)) with [PtCl$_2$(bpy)] also give the dinuclear complexes, [Pt(bpy){M(aet)$_3$}]$^{2+}$. While the reaction of *fac*(*S*)-[Co(aet)$_3$] with [PtCl$_2$(bpy)] is accompanied by isomerization from *fac*(*S*)-[Co(aet)$_3$] to *mer*(*S*)-[Co(aet)$_3$], no isomerization takes place in the reaction between *fac*(*S*)-[Rh(aet)$_3$] with [PtCl$_2$(bpy)]. This implies that *fac*(*S*)-[Co(aet)$_3$] is structurally more flexible compared with *fac*(*S*)-[Rh(aet)$_3$]. Although *fac*(*S*)-[M(aet)$_3$] (M = Co^{III} or Rh^{III}) possesses three available S atoms to be bound to another metal ions, it functions as bidentate ligands for [PtCl$_2$(bpy)] with two susceptible sites to substitution of other ligands, as in the case of *cis*(*S*)-[Co(aet)$_2$(en)]$^+$ units in [Ni{Co(aet)$_2$(en)}$_2$]$^{4+}$. Consequently, the produced dinuclear complex, [Pt(bpy){M(aet)$_3$}]$^{2+}$, has one non-bridging S atom. As mentioned later, the non-bridging S atoms of [M(aet)$_3$] in [Pt(bpy){M(aet)$_3$}]$^{2+}$ are electrochemically distinguishable between the cases of M = Co^{III} and Rh^{III}. This may indicate the differences of reactivities between the complexes **2** and **3**. In order to pursue this point, we tried the methylations of complexes **2** and **3** by the reaction of [Pt(bpy){M(aet)$_3$}]$^{2+}$ with dimethyl sulfate. The reaction of **2** with dimethyl sulfate gave a methylated complex, [Pt(bpy){Co(aet)$_2$(smaet)}]$^{3+}$ (**4**), but no methylated complex of **3** was obtained under any conditions. These facts support the different reactivities between complexes **2** and **3**, as mentioned above. These distinguishable reactivities are considered to be mainly due to a steric effect around a non-bridging S atom and/or M–S bond strength.

X-Ray Crystal Structures. An X-ray structural analysis for **1**·(NO$_3$)$_3$·1.75H$_2$O revealed the presence of a discrete trivalent complex cation, three nitrate anions, and one and three quarters water molecules. Similarly, **2**·(NO$_3$)$_2$·1.5H$_2$O consists of a discrete divalent complex cation, two nitrate anions, and one and a half water molecules. On the other hand, **3**·Br$_2$·5.5H$_2$O contains two independent divalent complex cations, four bromide anions, and eleven water molecules. Perspective drawings of the complex cations **1**, **2**, and **3** are given in Figs. 1, 2, and 3, respectively. Their selected bond distances and angles are listed in Tables 5, 6, and 7.

As shown in Figs. 1 and 2, both complex cations **1** and **2** contain one Co atom and one Pt atom to form the dinuclear complex. The Co atom in **1** is surrounded by two aet ligands and one en ligand to have an approximately octahedral geometry. Its equatorial coordination sites are occupied by two S atoms in aet and two N atoms in en, and the axial ones by two N atoms in aet, forming C_2 symmetrical *cis*(*S*)-[Co(aet)$_2$(en)]$^+$ unit. On the other hand, the Co atom in **2** is surrounded by the three aet ligands, and also has an

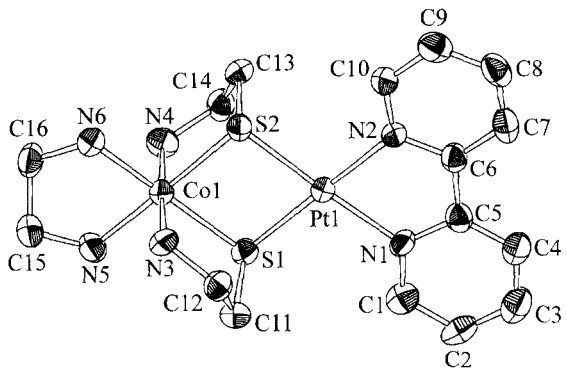

Fig. 1. Perspective view of [Pt(bpy){Co(aet)$_2$(en)}]$^{3+}$ (**1**) with the atomic labeling scheme.

Table 2. Final Atomic Coordinates and Equivalent Isotropic Thermal Parameters (B_{eq}/Å)[a] for [Pt(bpy){Co(aet)$_2$(en)}](NO$_3$)$_3$·1.75H$_2$O (**1**)

Atom	x	y	z	B_{eq}
Pt(1)	0.01731(1)	0.348552(9)	0.58937(1)	2.598(4)
Co(1)	0.06757(4)	0.20453(3)	0.53472(5)	2.46(1)
S(1)	−0.03612(8)	0.25032(7)	0.56929(10)	2.84(3)
S(2)	0.12443(8)	0.29919(6)	0.56661(10)	2.90(3)
O(1)	0.0828(3)	0.3467(2)	0.3273(4)	5.4(1)
O(2)	0.2015(3)	0.3663(2)	0.3240(4)	5.5(1)
O(3)	0.1764(3)	0.2807(2)	0.3809(3)	5.0(1)
O(4)	0.0980(5)	0.1599(3)	0.2762(4)	8.7(2)
O(5)	0.1151(3)	0.1084(3)	0.1637(3)	6.3(1)
O(6)	0.1888(3)	0.0912(3)	0.3019(4)	7.4(2)
O(7)	0.1327(5)	−0.1089(5)	0.4458(6)	14.2(3)
O(8)	0.2017(5)	−0.1119(4)	0.3484(6)	12.5(2)
O(9)	0.2122(7)	−0.1681(6)	0.4523(7)	16.1(4)
O(10)	0.1131(5)	0.0311(3)	0.6816(5)	8.4(2)
O(11)[b]	1.0000	0.1243(4)	0.7500	6.9(2)
O(12)[c]	0.126(2)	0.056(1)	0.870(2)	9.3(8)
N(1)	−0.0761(2)	0.3976(2)	0.6097(3)	2.80(9)
N(2)	0.0647(3)	0.4364(2)	0.6078(3)	2.66(9)
N(3)	0.0139(3)	0.2273(2)	0.4028(3)	2.93(9)
N(4)	0.1206(3)	0.1840(2)	0.6677(3)	3.27(10)
N(5)	0.0202(3)	0.1192(2)	0.5131(3)	3.3(1)
N(6)	0.1567(3)	0.1678(2)	0.4983(3)	3.15(10)
N(7)	0.1524(3)	0.3316(2)	0.3435(3)	3.28(10)
N(8)	0.1344(3)	0.1202(2)	0.2486(4)	3.8(1)
N(9)	0.1710(5)	−0.1153(5)	0.4059(5)	9.2(2)
C(1)	−0.1468(4)	0.3736(3)	0.6120(4)	3.6(1)
C(2)	−0.2047(3)	0.4108(3)	0.6277(4)	4.0(1)
C(3)	−0.1915(4)	0.4726(3)	0.6430(4)	4.1(1)
C(4)	−0.1200(4)	0.4978(3)	0.6402(4)	3.5(1)
C(5)	−0.0623(3)	0.4593(3)	0.6252(4)	3.0(1)
C(6)	0.0160(3)	0.4813(2)	0.6216(4)	2.9(1)
C(7)	0.0411(4)	0.5427(3)	0.6327(4)	3.7(1)
C(8)	0.1157(4)	0.5579(3)	0.6305(4)	4.1(1)
C(9)	0.1646(4)	0.5124(3)	0.6151(4)	3.9(1)
C(10)	0.1374(4)	0.4515(3)	0.6042(4)	3.4(1)
C(11)	−0.1039(3)	0.2523(3)	0.4497(4)	3.6(1)
C(12)	−0.0565(4)	0.2686(3)	0.3842(4)	3.3(1)
C(13)	0.1867(3)	0.2846(3)	0.6864(4)	3.6(1)
C(14)	0.1459(4)	0.2381(3)	0.7312(4)	3.6(1)
C(15)	0.0645(4)	0.0808(3)	0.4618(4)	3.9(1)
C(16)	0.1516(4)	0.0988(3)	0.5013(4)	3.8(1)

a) B_{eq} denotes the equivalent isotropic temperature factors, $B_{eq} = (8\pi^2/3)\sum_i\sum_j U_{ij}a_i^*a_j^*\boldsymbol{a}_i\cdot\boldsymbol{a}_j$. b) Occupancy factor = 0.50. c) Occupancy factor = 0.25.

Table 3. Final Atomic Coordinates and Equivalent Isotropic Thermal Parameters (B_{eq}/Å) [a] for [Pt(bpy){Co(aet)$_3$}](NO$_3$)$_2$·1.5H$_2$O (**2**)

Atom	x	y	z	B_{eq}
Pt(1)	0.11974(2)	0.29426(2)	0.03087(3)	2.638(4)
Co(1)	0.21723(7)	0.12870(5)	−0.2197(1)	2.55(2)
S(1)	0.2726(1)	0.2815(1)	−0.1140(2)	2.99(3)
S(2)	0.0806(1)	0.1369(1)	−0.0502(2)	3.17(3)
S(3)	0.1652(2)	−0.0237(1)	−0.3089(2)	3.41(3)
O(1)	0.5425(6)	0.0592(5)	0.835(1)	7.8(2)
O(2)	0.5985(8)	0.1951(5)	0.793(1)	8.8(2)
O(3)	0.7166(6)	0.1000(6)	0.872(1)	8.0(2)
O(4)	0.2909(6)	0.3014(4)	0.4411(7)	6.1(2)
O(5)	0.2954(6)	0.4496(4)	0.510(1)	7.1(2)
O(6)	0.1447(6)	0.3599(4)	0.5196(8)	5.5(1)
O(7)	0.565(1)	0.2550(9)	0.457(1)	13.3(4)
O(8)[b]	0.503(2)	0.438(2)	0.377(5)	23.3(9)
N(1)	0.1531(5)	0.4345(3)	0.1100(6)	3.0(1)
N(2)	−0.0221(5)	0.3150(3)	0.1481(6)	2.8(1)
N(3)	0.3252(5)	0.0933(4)	−0.0305(7)	3.4(1)
N(4)	0.1058(5)	0.1620(3)	−0.4101(7)	3.1(1)
N(5)	0.3340(5)	0.1291(4)	−0.3772(7)	3.2(1)
N(6)	0.6221(6)	0.1196(5)	0.8344(8)	4.1(1)
N(7)	0.2462(6)	0.3707(4)	0.4906(8)	4.4(1)
C(1)	0.2472(6)	0.4898(5)	0.0861(9)	3.6(1)
C(2)	0.2653(8)	0.5829(5)	0.147(1)	4.7(2)
C(3)	0.1828(8)	0.6212(5)	0.229(1)	4.6(2)
C(4)	0.0867(7)	0.5643(4)	0.2523(9)	3.8(1)
C(5)	0.0729(6)	0.4697(4)	0.1906(8)	3.1(1)
C(6)	−0.0234(6)	0.4052(4)	0.2111(8)	3.0(1)
C(7)	−0.1175(7)	0.4287(5)	0.2892(9)	3.9(1)
C(8)	−0.2071(7)	0.3610(5)	0.2995(10)	4.2(2)
C(9)	−0.2020(7)	0.2708(5)	0.2369(10)	4.0(2)
C(10)	−0.1069(7)	0.2505(5)	0.1616(9)	3.8(1)
C(11)	0.3895(6)	0.2590(5)	0.0486(9)	3.7(1)
C(12)	0.3627(7)	0.1660(5)	0.1162(9)	3.9(2)
C(13)	−0.0388(6)	0.1293(5)	−0.2247(10)	4.0(2)
C(14)	−0.0019(6)	0.1891(5)	−0.360(1)	4.1(2)
C(15)	0.2911(7)	−0.0404(5)	−0.412(1)	4.6(2)
C(16)	0.3213(7)	0.0442(5)	−0.5001(10)	4.3(2)

a) B_{eq} denotes the equivalent isotropic temperature factors, $B_{eq} = (8\pi^2/3)\sum_i\sum_j U_{ij}a_i^*a_j^*\boldsymbol{a}_i\cdot\boldsymbol{a}_j$. b) Occupancy factor = 0.5.

approximately octahedral geometry. The equatorial coordination sites are occupied by three S atoms and one N atom, and the axial ones by two N atoms in aet, forming *mer*(*S*)-[Co(aet)$_3$] unit. This indicates that the starting *fac*(*S*) isomer isomerizes to *mer*(*S*) isomer. The Pt atom in **1** or **2** is coordinated by two N atoms in bpy and two S atoms from C_2-*cis*(*S*)-[Co(aet)$_2$(en)]$^+$ or *mer*(*S*)-[Co(aet)$_3$] unit, both having a square-planar geometry. The Co(III) equatorial plane and the Pt^{II}S$_2$N$_2$ plane in **1** and **2** are essentially coplanar (dihedral angles; 6.23° for **1**, 8.78° for **2**), and their Co–Pt distance are 3.3880(7) and 3.3820(8) Å, respectively. The S–Pt–S angles in **1** (82.84(5)°) and **2** (83.53(6)°) are relatively acute compared with that observed in [Pt(bpy){Ni(aet)$_2$(bpy)}]$^{2+}$ (87.46(5)°).[18] Though the N–Pt–N angle (79.5(2)°) in **1** almost corresponds to that (79.4(2)°) in **2**, the Pt–N distances (av. 2.050(5) Å) in former is slightly shorter than that (av. 2.062(5) Å) in latter. On the other hand, the Pt–S distances (av. 2.284 (2) Å) in **1** are slightly shorter than those (av. 2.294(2) Å) in **2**, which correspond well to the Pt–S distances (av. 2.297(2) Å) in [Pt(bpy){Ni(aet)$_2$(bpy)}]$^{2+}$.[18] The Co–S1 distance bonded *trans* to the S3 atom in **2** is 2.297(2) Å and the average *cis* Co–S distance in **1** and **2** is 2.256(2) Å. A difference between the *trans* and *cis* Co–S distances, 0.041 Å indicates the *trans* influence due to the coordinated S atom, as in the case of the Co(III) complexes with the thiolato ligands such as L-penicillaminate and aminoethanethiolate.[19]

In the crystal of **3**·Br$_2$·5.5H$_2$O, which consists of two in-

Table 4. Final Atomic Coordinates and Equivalent Isotropic Thermal Parameters (B_{eq}/Å) [a] for $[Pt(bpy)\{Rh(aet)_3\}]Br_2 \cdot 5.5H_2O$ (**3**)

Atom	x	y	z	B_{eq}	Atom	x	y	z	B_{eq}
Pt(1)	−0.15872(2)	0.41942(3)	0.45238(1)	2.385(6)	N(9)	0.2957(6)	−0.0247(6)	0.7029(3)	3.5(2)
Pt(2)	0.10982(2)	0.08009(3)	0.57480(1)	2.733(7)	N(10)	0.2727(6)	0.1747(6)	0.7345(3)	3.5(2)
Rh(1)	−0.33760(5)	0.39305(5)	0.36552(2)	2.55(1)	C(1)	−0.1925(6)	0.4066(7)	0.5530(3)	3.1(2)
Rh(2)	0.27055(5)	0.10898(5)	0.66909(3)	2.63(1)	C(2)	−0.1684(8)	0.3938(9)	0.6013(3)	4.5(3)
Br(1)	−0.37635(10)	0.5808(1)	0.56971(5)	6.53(4)	C(3)	−0.0767(8)	0.3672(8)	0.6187(4)	4.3(3)
Br(2)	−0.54491(9)	0.47495(10)	0.77205(4)	5.06(3)	C(4)	−0.0141(7)	0.3575(8)	0.5885(3)	3.5(2)
Br(3)	−0.11190(10)	0.6054(1)	0.69362(5)	6.15(4)	C(5)	−0.0429(6)	0.3714(7)	0.5405(3)	2.8(2)
Br(4)	−0.3746(1)	0.2825(1)	0.68198(8)	9.26(6)	C(6)	0.0185(6)	0.3684(6)	0.5062(3)	2.3(2)
S(1)	−0.3188(2)	0.4328(2)	0.44464(8)	2.86(5)	C(7)	0.1127(6)	0.3403(7)	0.5163(3)	3.2(2)
S(2)	−0.1919(2)	0.4597(2)	0.37389(8)	2.93(5)	C(8)	0.1658(6)	0.3412(7)	0.4820(4)	3.7(2)
S(3)	−0.2827(2)	0.2403(2)	0.38438(9)	3.33(5)	C(9)	0.1273(6)	0.3685(7)	0.4367(3)	3.4(2)
S(4)	0.2624(2)	0.0362(2)	0.59680(8)	3.16(5)	C(10)	0.0332(6)	0.3937(7)	0.4279(3)	2.9(2)
S(5)	0.1152(2)	0.0686(2)	0.65585(8)	2.92(5)	C(11)	−0.3485(7)	0.5605(8)	0.4354(4)	3.7(2)
S(6)	0.2322(2)	0.2597(2)	0.63805(9)	3.29(5)	C(12)	−0.4265(7)	0.5696(7)	0.3942(4)	3.6(2)
O(1)	−0.6776(6)	0.4323(7)	0.8497(3)	6.7(3)	C(13)	−0.1530(7)	0.3842(9)	0.3299(3)	3.9(2)
O(2)	−0.2825(7)	0.7451(7)	0.6434(4)	7.6(3)	C(14)	−0.2287(7)	0.3928(9)	0.2858(3)	4.1(2)
O(3)	−0.3717(6)	0.5142(6)	0.6878(3)	5.5(2)	C(15)	−0.387(1)	0.195(1)	0.4000(7)	9.4(5)
O(4)	0.0266(8)	0.7802(8)	0.7360(5)	10.7(4)	C(16)	−0.4689(8)	0.2369(10)	0.3793(6)	7.0(4)
O(5)	0.1556(8)	0.7170(8)	0.8106(4)	8.4(3)	C(17)	0.1684(7)	0.0908(7)	0.4776(3)	3.6(2)
O(6)	−0.5133(7)	0.2518(7)	0.7571(3)	7.2(3)	C(18)	0.1580(9)	0.1102(9)	0.4311(4)	5.1(3)
O(7)	0.1493(7)	0.5258(8)	0.8214(3)	7.9(3)	C(19)	0.0720(9)	0.1425(9)	0.4087(4)	4.8(3)
O(8)	0.0457(7)	0.4513(8)	0.7416(4)	7.6(3)	C(20)	0.0018(8)	0.1515(8)	0.4336(3)	4.0(2)
O(9)	−0.609(1)	0.472(2)	0.9484(5)	19.0(7)	C(21)	0.0163(7)	0.1294(7)	0.4814(3)	3.2(2)
O(10)	−0.447(2)	0.755(1)	0.4989(6)	21.3(7)	C(22)	−0.0554(7)	0.1349(7)	0.5113(3)	3.0(2)
O(11)[b]	0.603(1)	0.233(3)	0.0630(7)	19(1)	C(23)	−0.1483(8)	0.1603(7)	0.4950(4)	4.0(2)
O(12)[b]	0.533(2)	0.087(2)	0.4962(9)	11.7(8)	C(24)	−0.2101(8)	0.1641(9)	0.5246(4)	5.3(3)
N(1)	−0.1316(5)	0.3977(5)	0.5235(3)	2.8(2)	C(25)	−0.1798(7)	0.1453(8)	0.5716(4)	4.1(2)
N(2)	−0.0182(5)	0.3940(5)	0.4612(3)	2.7(2)	C(26)	−0.0895(7)	0.1183(8)	0.5867(4)	4.0(2)
N(3)	−0.3972(5)	0.5302(6)	0.3517(3)	3.6(2)	C(27)	0.3512(7)	0.1105(9)	0.5775(4)	4.1(2)
N(4)	−0.3213(6)	0.3629(6)	0.2956(3)	3.4(2)	C(28)	0.4330(7)	0.1056(9)	0.6176(4)	4.6(3)
N(5)	−0.4689(5)	0.3292(6)	0.3609(3)	3.7(2)	C(29)	0.1323(7)	−0.0569(8)	0.6724(3)	3.7(2)
N(6)	0.1010(6)	0.1002(5)	0.5037(3)	3.0(2)	C(30)	0.2105(8)	−0.0666(7)	0.7144(4)	4.0(2)
N(7)	−0.0273(5)	0.1141(5)	0.5574(3)	3.0(2)	C(31)	0.1870(10)	0.3043(9)	0.6886(4)	5.4(3)
N(8)	0.4094(5)	0.1392(6)	0.6632(3)	3.6(2)	C(32)	0.2441(10)	0.2733(8)	0.7331(4)	5.4(3)

a) B_{eq} denotes the equivalent isotropic temperature factors, $B_{eq} = (8\pi^2/3)\sum_i\sum_j a_i^* a_j^* \boldsymbol{a}_i \cdot \boldsymbol{a}_j$. b) Occupancy factor = 0.5.

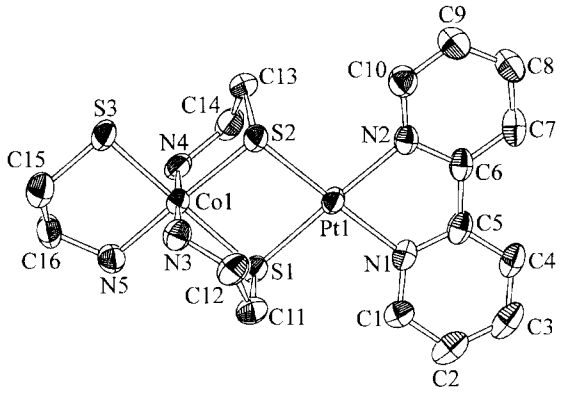

Fig. 2. Perspective view of $[Pt(bpy)\{Co(aet)_3\}]^{2+}$ (**2**) with the atomic labeling scheme.

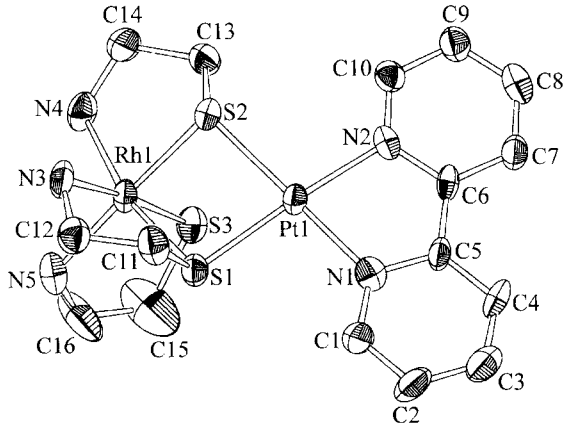

Fig. 3. Perspective view of $[Pt(bpy)\{Rh(aet)_3\}]^{2+}$ (**3**) with the atomic labeling scheme.

dependent divalent complex cations, the structures of both cations are almost the same as each other (Table 7), except for the absolute configurations in octahedral Rh units, and only one isomer has been shown in Fig. 3. Each Rh atom is coordinated by three aet ligands to have an essentially octahedral geometry, which is a similar structure to the corresponding Co(III) units in **1** and **2**. In contrast to **2**, however, the equatorial coordination sites of the Rh(III) unit are occupied by two S and two N atoms in aet, and the axial sites are filled

Table 5. Selected Bond Distances (Å) and Angles (deg) of [Pt(bpy){Co(aet)$_2$(en)}](NO$_3$)$_3$·1.75H$_2$O (**1**)

Pt(1)–S(1)	2.293(1)	Pt(1)–S(2)	2.276(2)
Pt(1)–N(1)	2.052(5)	Pt(1)–N(2)	2.049(4)
Co(1)–S(1)	2.267(2)	Co(1)–S(2)	2.253(2)
Co(1)–N(3)	1.977(4)	Co(1)–N(4)	1.978(4)
Co(1)–N(5)	2.000(5)	Co(1)–N(6)	1.975(5)
S(1)–Pt(1)–S(2)	82.84(5)	S(1)–Pt(1)–N(1)	100.3(1)
S(1)–Pt(1)–N(2)	179.7(1)	S(2)–Pt(1)–N(1)	176.9(1)
S(2)–Pt(1)–N(2)	97.4(1)	N(1)–Pt(1)–N(2)	79.5(2)
S(1)–Co(1)–S(2)	83.96(6)	S(1)–Co(1)–N(3)	87.2(2)
S(1)–Co(1)–N(4)	91.7(2)	S(1)–Co(1)–N(5)	96.4(2)
S(1)–Co(1)–N(6)	176.7(1)	S(2)–Co(1)–N(3)	92.0(1)
S(2)–Co(1)–N(4)	86.9(1)	S(2)–Co(1)–N(5)	177.0(1)
S(2)–Co(1)–N(6)	94.7(1)	N(3)–Co(1)–N(4)	178.5(2)
N(3)–Co(1)–N(5)	91.0(2)	N(3)–Co(1)–N(6)	89.9(2)
N(4)–Co(1)–N(5)	90.2(2)	N(4)–Co(1)–N(6)	91.2(2)
N(5)–Co(1)–N(6)	85.1(2)	Pt(1)–S(1)–Co(1)	95.98(6)
Pt(1)–S(2)–Co(1)	96.84(6)		

Table 6. Selected Bond Distances (Å) and Angles (deg) of [Pt(bpy){Co(aet)$_3$}](NO$_3$)$_2$·1.5H$_2$O (**2**)

Pt(1)–S(1)	2.290(2)	Pt(1)–S(2)	2.297(2)
Pt(1)–N(1)	2.057(5)	Pt(1)–N(2)	2.066(5)
Co(1)–S(1)	2.297(2)	Co(1)–S(2)	2.247(2)
Co(1)–S(3)	2.258(2)	Co(1)–N(3)	1.959(6)
Co(1)–N(4)	1.978(5)	Co(1)–N(5)	1.987(6)
S(1)–Pt(1)–S(2)	83.53(6)	S(1)–Pt(1)–N(1)	97.8(2)
S(1)–Pt(1)–N(2)	175.0(1)	S(2)–Pt(1)–N(1)	178.4(2)
S(2)–Pt(1)–N(2)	99.4(1)	N(1)–Pt(1)–N(2)	79.4(2)
S(1)–Co(1)–S(2)	84.50(6)	S(1)–Co(1)–S(3)	176.89(7)
S(1)–Co(1)–N(3)	87.4(2)	S(1)–Co(1)–N(4)	93.6(1)
S(1)–Co(1)–N(5)	93.2(2)	S(2)–Co(1)–S(3)	94.11(7)
S(2)–Co(1)–N(3)	91.1(2)	S(2)–Co(1)–N(4)	88.2(2)
S(2)–Co(1)–N(5)	176.0(2)	S(3)–Co(1)–N(3)	89.9(2)
S(3)–Co(1)–N(4)	89.1(1)	S(3)–Co(1)–N(5)	88.3(2)
N(3)–Co(1)–N(4)	178.7(2)	N(3)–Co(1)–N(5)	92.1(2)
N(4)–Co(1)–N(5)	88.7(2)	Pt(1)–S(1)–Co(1)	95.00(6)
Pt(1)–S(2)–Co(1)	96.18(6)		

Table 7. Selected Bond Distances (Å) and Angles (deg) of [Pt(bpy){Rh(aet)$_3$}]Br$_2$·5.5H$_2$O (**3**)

Pt(1)–S(1)	2.317(2)	Pt(1)–S(2)	2.300(2)
Pt(1)–N(1)	2.040(8)	Pt(1)–N(2)	2.056(7)
Pt(2)–S(4)	2.295(3)	Pt(2)–S(5)	2.325(2)
Pt(2)–N(6)	2.047(8)	Pt(2)–N(7)	2.037(8)
Rh(1)–S(1)	2.315(2)	Rh(1)–S(2)	2.301(3)
Rh(1)–S(3)	2.336(3)	Rh(1)–N(3)	2.136(9)
Rh(1)–N(4)	2.110(8)	Rh(1)–N(5)	2.101(8)
Rh(2)–S(4)	2.305(3)	Rh(2)–S(5)	2.306(2)
Rh(2)–S(6)	2.343(3)	Rh(2)–N(8)	2.106(8)
Rh(2)–N(9)	2.130(8)	Rh(2)–N(10)	2.094(8)
S(1)–Pt(1)–S(2)	81.00(8)	S(1)–Pt(1)–N(1)	97.5(2)
S(1)–Pt(1)–N(2)	174.4(2)	S(2)–Pt(1)–N(1)	174.2(2)
S(2)–Pt(1)–N(2)	101.9(2)	N(1)–Pt(1)–N(2)	80.2(3)
S(4)–Pt(2)–S(5)	80.67(8)	S(4)–Pt(2)–N(6)	102.0(2)
S(4)–Pt(2)–N(7)	177.2(2)	S(5)–Pt(2)–N(6)	175.7(2)
S(5)–Pt(2)–N(7)	97.4(2)	N(6)–Pt(2)–N(7)	80.1(3)
S(1)–Rh(1)–S(2)	81.01(8)	S(1)–Rh(1)–S(3)	91.00(9)
S(1)–Rh(1)–N(3)	86.5(2)	S(1)–Rh(1)–N(4)	166.7(2)
S(1)–Rh(1)–N(5)	97.0(2)	S(2)–Rh(1)–S(3)	94.60(9)
S(2)–Rh(1)–N(3)	89.2(2)	S(2)–Rh(1)–N(4)	86.1(2)
S(2)–Rh(1)–N(5)	177.4(2)	S(3)–Rh(1)–N(3)	175.0(2)
S(3)–Rh(1)–N(4)	86.8(2)	S(3)–Rh(1)–N(5)	83.7(2)
N(3)–Rh(1)–N(4)	96.6(3)	N(3)–Rh(1)–N(5)	92.3(3)
N(4)–Rh(1)–N(5)	95.8(3)	S(4)–Rh(2)–S(5)	80.85(9)
S(4)–Rh(2)–S(6)	95.16(9)	S(4)–Rh(2)–N(8)	85.5(2)
S(4)–Rh(2)–N(9)	89.6(2)	S(4)–Rh(2)–N(10)	177.9(2)
S(5)–Rh(2)–S(6)	89.87(9)	S(5)–Rh(2)–N(8)	165.8(2)
S(5)–Rh(2)–N(9)	86.8(2)	S(5)–Rh(2)–N(10)	97.1(2)
S(6)–Rh(2)–N(8)	87.5(2)	S(6)–Rh(2)–N(9)	173.6(2)
S(6)–Rh(2)–N(10)	84.5(2)	N(8)–Rh(2)–N(9)	97.1(3)
N(8)–Rh(2)–N(10)	96.5(3)	N(9)–Rh(2)–N(10)	90.5(3)
Pt(1)–S(1)–Rh(1)	91.41(8)	Pt(1)–S(2)–Rh(1)	92.21(9)
Pt(2)–S(4)–Rh(2)	91.59(9)	Pt(2)–S(5)–Rh(2)	90.80(9)

by one S and one N atoms, forming *fac*(*S*)-[Rh(aet)$_3$] unit. This means that the Rh units retain their configuration during the reaction. The Pt atom is coordinated by two N atoms in bpy and two S atoms from *fac*(*S*)-[Rh(aet)$_3$] unit, which apparently shows a square-planar geometry. The Rh–S–Pt bridging angles (av. 91.50(9)°) are relatively acute compared with the Rh–S–M ones in **1** (M = Co, av. 96.41(6)°) and **2** (M = Co, av. 95.59(6)°), and that (M = Ni, av. 95.46(6)°) in [Pt(bpy){Ni(aet)$_2$(bpy)}]$^{2+}$.[18] Furthermore, the RhN$_2$S$_2$ equatorial plane in **3** is considerably (av. 20.32°) bent for the PtS$_2$N$_2$ plane (Fig. 3), and the Rh–Pt distance (av. 3.3066(8) Å) are shorter than M–Pt distances in **1** (3.3880(7) Å) and **2** (3.3820(8) Å). The distance between the S atom on the axial site of Rh(III) unit and the Pt atom is av. 3.476(3) Å and the corresponding distance between the N atom on the other site of Rh(III) unit and the Pt atom is av. 4.432(7) Å. These facts may suggest that there is weak interaction between the thiolato sulfur atom of the Rh(III) unit and the vacant axial site of the Pt atom.

It is noted that **1** exists in the linear-chain-like structure with an alternate coplanar stacking arrangement, in which the {Pt(bpy)} moieties of the neighboring complex cations are antiparallel to each other (Fig. 4). The interplane distances between the neighboring {Pt(bpy)} moieties in **1** are of the av. 3.572 Å, and are within the range of the π–π stacking contact.[20] On the other hand, **2** exists in the dimeric form with the edge-to-edge type π–π interactions (Fig. 5), that is, the N2, C1, and C5 atoms in one complex cation are close to the C3, C7, and C5 atoms in the adjacent complex cation, respectively (N2–C3 = 3.536(9), C1–C7 = 3.48(1), C5–C5 = 3.47(1) Å). In this structure, one vacant axial site of the Pt atom seems to be occupied by the oxygen atom of one nitrate anion (Pt–O = 3.562(6) Å). This indicates an interaction between the Pt and O atoms. Similarly to the case of **1**, **3** exists in the linear-chain-like structure with an alternate coplanar stacking arrangement (Fig. 6). Namely, the interplane distances (av. 3.420 Å) between the neighboring {Pt(bpy)} moieties in **3** are also within the range of the π–π

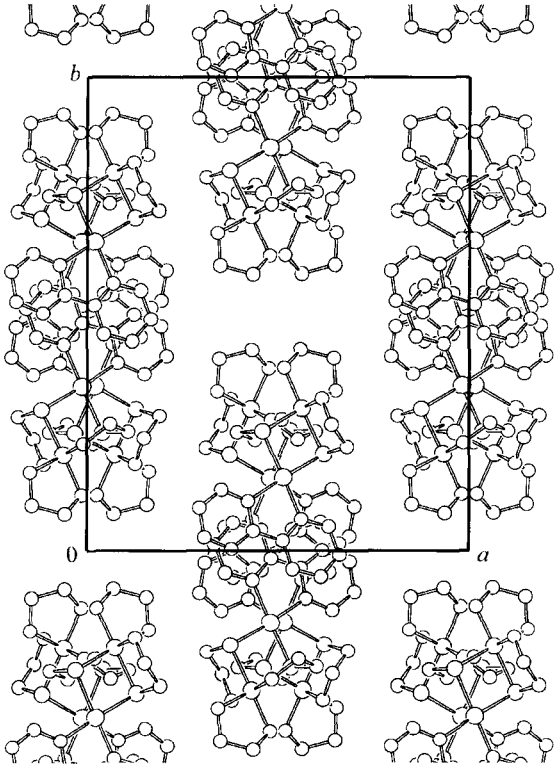

Fig. 4. Projection of crystal packing for $[Pt(bpy)\{Co(aet)_2(en)\}]^{3+}$ (**1**) viewed along *c* axis.

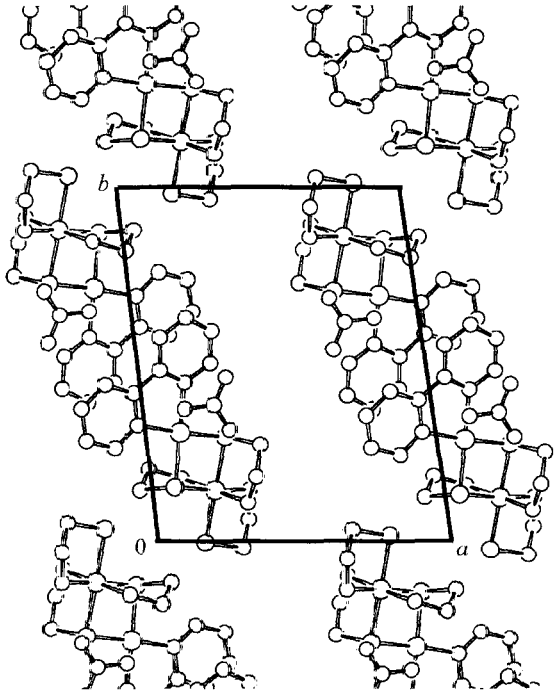

Fig. 5. Projection of crystal packing for $[Pt(bpy)\{Co(aet)_3\}]^{2+}$ (**2**) viewed along *c* axis.

stacking contact.[20]

There are two possible optical isomers, Δ and Λ, for **1** and **2**, considering the absolute configurations of the octahedral Co(III) units. In crystals, **1** and **2** exist as the racemate, as shown in the crystal systems (Table 1). Both of two bridging sulfur atoms in **1** and **2** are fixed to the *S* configuration for the Δ isomer and the *R* configuration for Λ isomer (Figs. 1 and 2). The Rh(1) and Rh(2) units have the Δ and Λ configurations, respectively, and both of two bridging sulfur atoms in **3** are fixed to the *R* configuration for the Δ isomer and the *S* configuration for Λ isomer.

Characterization. The electronic absorption and CD spectra of **1**, **2**, and **3** are shown in Fig. 7, and the data are summarized in Table 8. The absorption spectral patterns of **1** and **2** are almost identical with each other over the whole region, although the first d–d absorption band of **2** (18.58×10^3 cm^{-1}) is more broadened and lowered than that of **1** (19.90×10^3 cm^{-1}). This will reflect that the coordination sphere of Co(III) ion in **2** is of the meridional configuration and its symmetry is lower than that of **1**. The absorption bands in the higher energy region are mainly due to the charge-transfer from μ-S to Co(III) or the localized transitions on bpy, and appear at almost the same wavenumber with the same intensities. While **3** shows the π–π^* bands

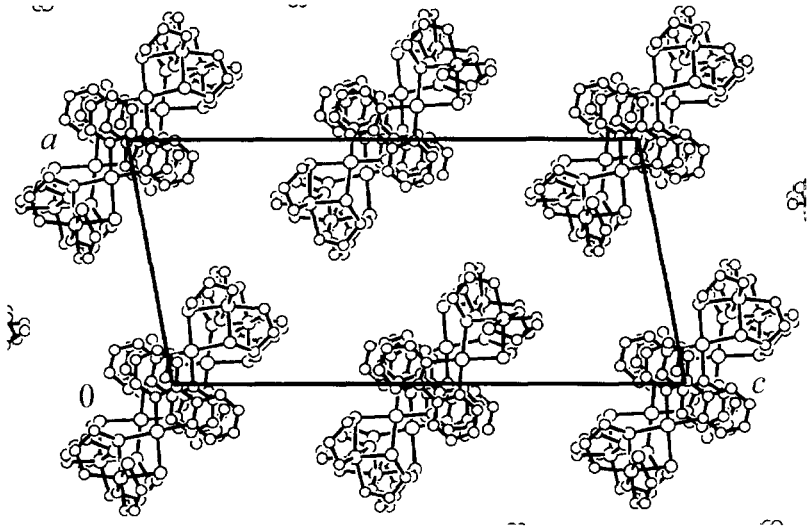

Fig. 6. Projection of crystal packing for $[Pt(bpy)\{Rh(aet)_3\}]^{2+}$ (**3**) viewed along *b* axis.

Table 8. Absorption and CD Spectral Data of $(+)^{CD}_{600}$-[Pt(bpy){Co(aet)$_2$(en)}]$^{3+}$ ($(+)^{CD}_{600}$-**1**), $(+)^{CD}_{600}$-[Pt(bpy){Co(aet)$_3$}]$^{2+}$ ($(+)^{CD}_{600}$-**2**), and $(+)^{CD}_{400}$-[Pt(bpy){Rh(aet)$_3$}]$^{2+}$ ($(+)^{CD}_{400}$-**3**) in H_2O

Absorption maxima $\sigma/10^3$ cm^{-1} (log ε/mol^{-1} dm^3 cm^{-1})		CD extrema $\sigma/10^3$ cm^{-1} ($\Delta\varepsilon$/mol^{-1} dm^3 cm^{-1})	
$(+)^{CD}_{600}$-[Pt(bpy){Co(aet)$_2$(en)}]$^{3+}$			
19.90	(2.37)	19.51	(+5.49)
25.2	(3.0)^{sh}	22.41	(+0.45)
29.4	(3.8)^{sh}	25.25	(+6.18)
31.31	(4.27)	30.74	(−9.26)
32.48	(4.25)	31.31	(−8.80)
39.6	(4.4)^{sh}	34.41	(−21.3)
42.6	(4.4)^{sh}	40.50	(+8.36)
48.8	(4.8)^{sh}	45.79	(+47.9)
		48.1	(+33)^{sh}
$(+)^{CD}_{600}$-[Pt(bpy){Co(aet)$_3$}]$^{2+}$			
18.58	(2.42)	17.82	(+4.53)
25.93	(3.7)^{sh}	21.85	(−1.46)
29.51	(4.2)^{sh}	25.37	(+5.39)
31.33	(4.46)	30.60	(−28.9)
32.34	(4.42)	37.37	(+13.4)
41.05	(4.41)	40.16	(+6.64)
49.0	(4.8)^{sh}	42.63	(+15)^{sh}
		44.92	(+22.0)
		45.29	(+21.9)
		48.69	(+52.6)
$(+)^{CD}_{400}$-[Pt(bpy){Rh(aet)$_3$}]$^{2+}$			
25.2	(2.7)^{sh}	25.25	(+2.04)
29.0	(3.7)^{sh}	29.20	(−9.23)
31.23	(4.19)	30.21	(−8.73)
32.26	(4.14)	30.63	(−9.20)
42.16	(4.60)	32.89	(+10.3)
48.0	(4.7)^{sh}	39.0	(−14)^{sh}
		41.69	(−41.5)
		43.86	(−16.5)
		47.62	(−43.8)

at 31.23 and 32.26×10^3 cm^{-1} localized on bpy are located at quite similar transition energies to those observed for **1** and **2**, or the other complexes with {Pt(bpy)} moiety,[18,21–24] the first (25.2×10^3 cm^{-1}) and second (29.0×10^3 cm^{-1}) d–d transition bands due to Rh(III) ion, and the charge-transfer band (42.16×10^3 cm^{-1}) from μ-S to Rh(III) appear at higher energy side than those of the corresponding bands for **1** and **2**. These results can be interpreted as the differences between Rh(III) and Co(III) ions in the octahedral units. All of **1**, **2**, and **3** show an intense band around 48×10^3 cm^{-1}, which can be regarded as sulfur-to-metal charge-transfer transition. **1**, **2**, and **3**, which have the chiral center, Δ or Λ, for the arrangements of the chelate rings of the octahedral unit, were optically resolved, and the CD spectra of the $(+)^{CD}_{600}$-**1**, $(+)^{CD}_{600}$-**2**, and $(+)^{CD}_{400}$-**3** isomers are illustrated in Fig. 7. The $(+)^{CD}_{600}$-**1** and $(+)^{CD}_{600}$-**2** isomers exhibit positive CD bands in the d–d transition region due to the Co(III) ion. These CD spectral patterns are the same as those of $\Lambda\Lambda$-[Ag$_3${Co(aet)$_3$}$_2$]$^{3+}$ and $\Lambda\Lambda\Lambda\Lambda$-[{Co(aet)$_3$}$_4Zn_4$O]$^{6+}$.[25,26] This indicates that both of the $(+)^{CD}_{600}$-**1** and $(+)^{CD}_{600}$-**2** isomers are assigned to have the Λ configurational for the Co(III) units. The CD spectral behavior in the d-d transition regions due to Rh(III) ion for the $(+)^{CD}_{400}$-**3** isomer is similar to those of the corresponding regions for the $(+)^{CD}_{600}$-**1** and $(+)^{CD}_{600}$-**2** isomers, although the CD bands of the Rh unit are shifted to higher energy side than those of the Co unit. Therefore, the $(+)^{CD}_{400}$-**3** isomer can be regarded as the Λ configurational for the Rh(III) unit. It is noted that **2** and **3** show opposite CD signs to each other in the wavenumber region of 44 to 50×10^3 cm^{-1}, in which the CT bands from μ-S to metal appear. Although both of **2** and **3** take Λ-configuration around the octahedral units, the X-ray analyses show that the μ-S atoms in **2** and **3** have *R* and *S* configurations, respectively. This will reflect the above different CD spectral behavior between **2** and **3**.

As shown in Fig. 8, the ^{13}C NMR spectrum of **1** with C_2 symmetry exhibits one signal due to the two methylene carbon atoms of en, two signals due to the four methylene carbons of aet, and five signals due to the ten carbon atoms of bpy. On the other hand, **2** shows sixteen independent signals, in which six signals are assigned to the six methylene carbons of aet and ten signals to the ten carbon atoms of

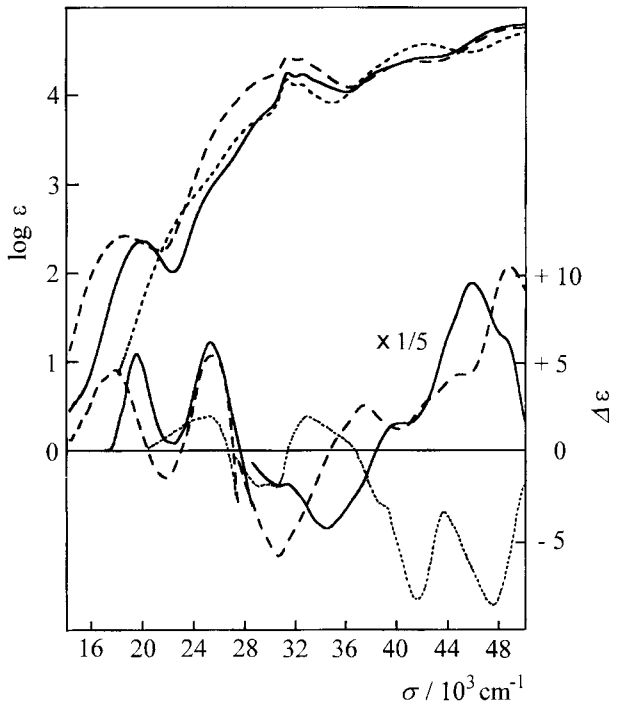

Fig. 7. Electronic absorption and CD spectra of $(+)^{CD}_{600}$-**1** (—), $(+)^{CD}_{600}$-**2** (- - -), and $(+)^{CD}_{400}$-**3** (····) in H_2O.

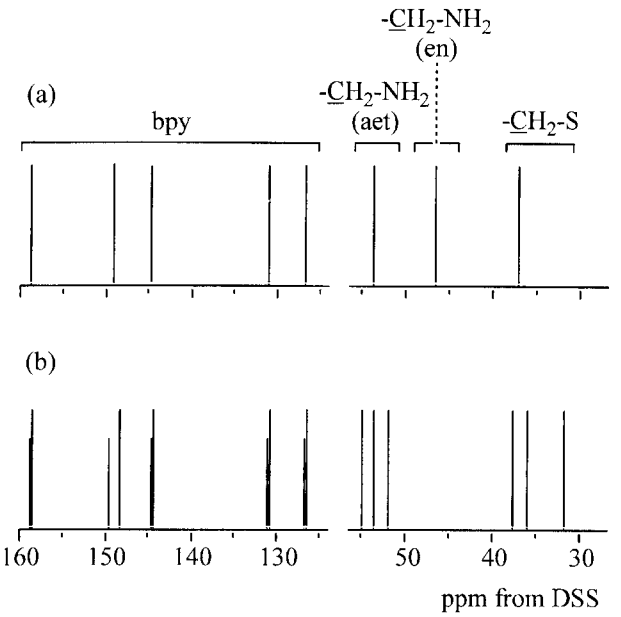

Fig. 8. ^{13}C NMR spectra of (a) $[Pt(bpy)\{Co(aet)_2(en)\}]^{3+}$ (**1**) and (b) $[Pt(bpy)\{Co(aet)_3\}]^{2+}$ (**2**) in D_2O.

bpy, because of the lower symmetry. Among these signals of **2**, those at the higher field (δ = 30—40 ppm) are due to the –S–CH_2– group in aet ligands, and the one at the highest field is assigned as the non-bridged S atom. The splitting of two sets of pyridyl carbons in bpy of **2**, contrasted with the case of **1**, is considered to be due to the lower symmetry. These imply that complexes **1** and **2** retain their structure in the aqueous solution, as in the solid state.

Electrochemical studies were performed for **1**, **2**, and **3** in 0.1 mol dm^{-3} sodium sulfate aqueous solutions. As shown in Fig. 9, the cyclic voltammogram at a glassy carbon electrode for **1** displays only one reversible redox couple ($E^{0'}$ = −0.52 V). Although **2** also displays a reversible redox couple ($E^{0'}$ = −0.76 V), the region is located at the more negative potential side than that of **1**. Except for the above redox couples, each of **1** and **2** shows no redox couples in the potential region of +0.5 to −1.0 V. Furthermore, a similar redox couple is observed in the case of $[Co\{Co(aet)_3\}_2]^{3+}$.[27] Accordingly, these reversible redox couples are assigned as Co(III)/Co(II) redox ones. This implies that the Co(III) atom is more stabilized in the N_3S_3 coordination sphere than in the N_4S_2 one. While **2** shows an electrochemically irreversible oxidation wave (E_{pa} = +0.90 V) besides the Co(III)/Co(II) redox process, no corresponding wave is observed in the case of **1**. This implies that the irreversible oxidation wave of **2** is considered to be due to the oxidation of the non-bridged S atom in the $[Co(aet)_3]$ unit. Furthermore, an irreversible reduction wave appears around −0.2 V after the oxidation process for **2**. This indicates that some oxidation product of **2** is formed after the oxidation. As for complex **3**, only one irreversible oxidation wave (E_{pa} = +0.75 V), which was assigned as the oxidation of the non-bridged S atom in the $[Rh(aet)_3]$ unit, was observed. In contrast with the oxidation of the non-bridged S atom in the *mer*(*S*)-$[Co(aet)_3]$ unit, the oxidation of the non-bridged S atom in *fac*(*S*)-$[Rh(aet)_3]$ gave three reduction waves in the potential region of +0.25 to −0.20 V. This implies that the oxidation of the non-bridged S atom of **3** gave some complicated oxidation product and/or decomposed species. Accordingly, these electrochemical

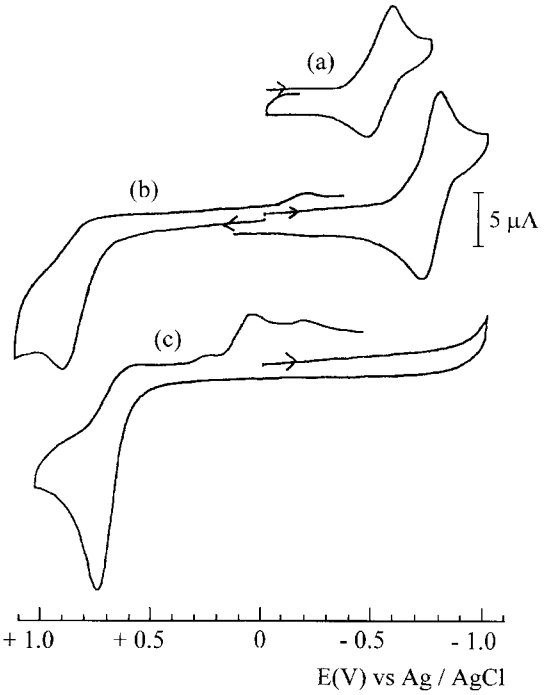

Fig. 9. Cyclic voltammograms of (a) $[Pt(bpy)\{Co(aet)_2(en)\}]^{3+}$ (**1**), (b) $[Pt(bpy)\{Co(aet)_3\}]^{2+}$ (**2**), and (c) $[Pt(bpy)\{Rh(aet)_3\}]^{2+}$ (**3**) in 0.1 mol dm^{-3} Na_2SO_4 aqueous solution.

experiments indicate some differences in the reactivities between the complexes **2** and **3**.

This work was partially supported by a Grant-in-Aid for Scientific Research No. 11640555 from the Ministry of Education, Science, Sports and Culture.

References

1 D. C. Jicha and D. H. Busch, *Inorg. Chem.*, **1**, 872 (1962).
2 D. C. Jicha and D. H. Busch, *Inorg. Chem.*, **1**, 884 (1962).
3 C. H. Wei and L. F. Dahl, *Inorg. Chem.*, **9**, 1878 (1970).
4 T. Konno, K. Yonenobu, J. Hidaka, and K. Okamoto, *Inorg. Chem.*, **33**, 861 (1994).
5 Y. Yamada and K. Okamoto, *Chem. Lett.*, **1999**, 315.
6 T. Konno, C. Sasaki, and K. Okamoto, *Chem. Lett.*, **1996**, 977.
7 K. Okamoto, C. Sasaki, Y. Yamada, and K. Konno, *Bull. Chem. Soc. Jpn.*, **72**, 1685 (1999).
8 T. Konno, J. Hidaka, and K. Okamoto, *Bull. Chem. Soc. Jpn.*, **68**, 1353 (1995).
9 T. Konno, J. Hidaka, and K. Okamoto, *Chem. Lett.*, **1996**, 975.
10 T. Konno, T. Machida, and K. Okamoto, *Bull. Chem. Soc. Jpn.*, **71**, 175 (1998).
11 N. Baidya, D. Ndreu, M. Olmstead, and K. Mascharak, *Inorg. Chem.*, **30**, 2448 (1991).
12 R. H. Herber, M. Croft, M. J. Coyer, B. Bilash, and A. Sahiner, *Inorg. Chem.*, **33**, 2422 (1994).
13 M. Kita, K. Yamanari, and Y. Shimura, *Bull. Chem. Soc. Jpn.*, **56**, 3272 (1983).
14 T. Konno, K. Okamoto, and J. Hidaka, *Inorg. Chem.*, **33**, 538 (1994).
15 Y. Miyashita, N. Sakagami, Y. Yamada, T. Konno, J. Hidaka, and K. Okamoto, *Bull. Chem. Soc. Jpn.*, **71**, 661 (1998).
16 "teXsan. Molecular Structure Corporation. Single Crystal Structure Analysis Software. Version 1.9," MSC, 3200 Research Forest Drive, The Woodlands, TX77381, USA (1998).
17 Lists of final atomic coordinates and equivalent isotropic thermal parameters for hydrogen atoms, anisotropic thermal parameters for non-hydrogen atoms, and bond distances and angles are deposited as Document No. 73023 at the Office of the Editor of Bull. Chem. Soc. Jpn.
18 K. Okamoto, Y. Yoshinari, Y. Yamada, N. Sakagami, and T. Konno, *Bull. Chem. Soc. Jpn.*, **71**, 1363 (1998).
19 K. Okamoto, H. Umehara, M. Nomoto, H. Einaga, and J. Hidaka, *Bull. Chem. Soc. Jpn.*, **60**, 1709 (1987).
20 W. B. Connick, R. E. Marsh, W. P. Schaefer, and H. B. Gray, *Inorg. Chem.*, **36**, 913 (1997).
21 E. Bielli, P. M. Gidney, R. D. Gillard, and B. T. Heaton, *J. Chem. Soc., Dalton Trans.*, **1974**, 2133.
22 S. S. Kamath, V. Uma, and T. S. Srivastava, *Inorg. Chim. Acta*, **161**, 49 (1989).
23 S. S. Kamath, V. Uma, and T. S. Srivastava, *Inorg. Chim. Acta*, **166**, 91 (1989).
24 M. Cusumano, M. L. D. Pietro, A. Giannetto, F. N.icolò and E. Rotondo, *Inorg. Chem.*, **37**, 563 (1998).
25 T. Konno, K. Okamoto, and J. Hidaka, *Inorg. Chem.*, **30**, 2253 (1991).
26 T. Konno, K. Tokuda, T. Suzuki, and K. Okamoto, *Bull. Chem. Soc. Jpn.*, **71**, 1049 (1998).
27 T. Konno, K. Nakamura, K. Okamoto, and J. Hidaka, *Bull. Chem. Soc. Jpn.*, **66**, 2582 (1993).